Long-Lived Population Inversion in Isovalently Doped Quantum Dots

Ohr Lahad,[†,§] Noga Meir,[†,§] Iddo Pinkas,[‡] and Dan Oron*[,†]

[†]Department of Physics of Complex Systems, Weizmann Institute of Science, Rehovot 7610001, Israel and [‡]Department of Chemical Research Support, Weizmann Institute of Science, Rehovot 7610001, Israel. [§]Ohr Lahad and Noga Meir contributed equally.

ABSTRACT Optical gain from colloidal quantum dots has been desired for several decades since their discovery. While gain from multiexcitations is by now well-established, nonradiative Auger recombination limits the lifetime of such population inversion in quantum dots. CdSe cores isovalently doped by one to few Te atoms capped with rod-shaped CdS are examined as a candidate system for enhanced stimulated emission properties. Emission depletion spectroscopy shows a behavior characteristic of 3-level gain systems in these quantum dots. This implies complete removal of the 2-fold degeneracy of the lowest energy electronic excitation due to the large repulsive exciton–exciton interaction in the doubly excited state. Using emission depletion measurements of the trap-associated emission from poorly passivated CdS quantum dots, we show that 3-level characteristics are typical of emission resulting from a band edge to trap state transition, but reveal subtle differences between the two systems. These results allow for unprecedented observation of long-lived population inversion from singly excited quantum dots.

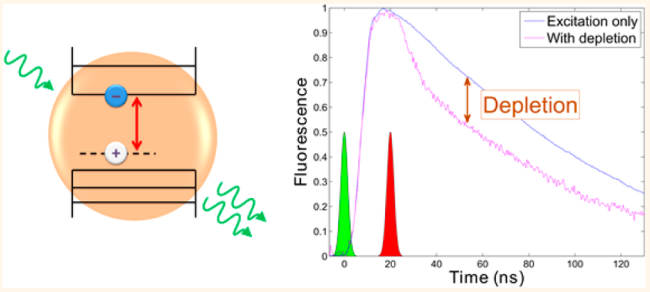

KEYWORDS: quantum dots · isovalent doping · trap emission · optical gain · stimulated emission

For the last two decades, significant efforts were invested in studying stimulated emission (SE) and attempting to achieve optical gain from colloidal semiconductor quantum dots (QDs).[1−6] The attractiveness of QD-based gain systems is partially due to the cost-effective solution processing, and partially due to the possibility to tune the emission wavelength from the ultraviolet to the near-infrared by tailoring the QD size[7] and composition. The improved temperature stability of QD and nanorod (NR)[8] devices further adds to make these systems desirable candidates for light amplification (see ref 9 and references therein). Yet, lasing and gain in QD-based systems have so far been significantly hindered due to the necessity to excite, at least partially, more than one exciton per QD to achieve population inversion. Most commonly (as in II–VI materials), excitation of biexcitons (BXs) is needed due to the 2-fold degeneracy of the lowest electronically excited state and the attractive interaction between multiple excitations in the same nanocrystal. The optical gain threshold is dictated by the detailed interplay between biexciton interaction and Stokes shifts.[10] The dynamics of these processes are discussed in a recent review.[11] Experimentally, the optical gain threshold in type-I QDs has been observed to be an average excitation level of $\langle N \rangle_{thr} \approx 1.6$.[12] While multiexcitons (MXs) provide the advantage of broad gain bandwidth,[13] the fast nonradiative Auger recombination of MXs[14] presents a main obstruction in realizing such amplification, typically allowing only for short-lived (<2 ns) optical gain. More recently, several authors have reported gain in the single exciton regime from QDs,[15−17] but none showed population inversion that is *long-lived* (*i.e.*, limited by the radiative lifetime of the singly excited state).

Super-resolution microscopy is another field which drew much attention to processes involving SE in the past two decades.[18] Reversible saturated switch-off of fluorophores allows imaging with subdiffraction limit resolution.[19] One successful method is stimulated emission depletion (STED), which relies on *full* inhibition of fluorescence by SE.[14] The high photostability and quantum yields (QYs) of QDs

* Address correspondence to dan.oron@weizmann.ac.il.

Received for review November 10, 2014 and accepted December 31, 2014.

Published online December 31, 2014
10.1021/nn506404n

compared to those of organic dye molecules, for which these methods are well-established, make QDs desirable candidates[20] for STED microscopy. Yet, because of the same restrictions, only a few implementations of light modulation have been reported with QDs,[21−24] and none showed full inhibition of fluorescence due to SE.

Type-II QDs, in which the electron and hole wave functions are spatially separated, have been suggested to allow for single exciton gain.[25] The separation of the charge carriers generates Coulomb repulsion between the two excitons comprising a BX. For a large enough blueshift of the BX state due to the Stark effect, photons resonant with the lowest single exciton transition will not be absorbed, and long-lived population inversion should be possible.

Large BX blueshifts have been observed in such Type-II QDs,[15] though the removal of the degeneracy was not complete. CdSe QDs isovalently doped with up to a few atoms of Te have shown, to date, the largest BX blueshifts.[26] In these systems, the hole wave function is strongly localized around the Te inclusion, leading to a very strong hole−hole repulsion in the biexciton state.[27] In addition, the large Stokes shift between the band-edge exciton and the Te-defect state simplifies the requirement for a low-energy transition which does not spectrally overlap with higher energy transitions. These two mechanisms practically suggest full removal of the lowest electronic state degeneracy and potential for stimulated emission in the single exciton regime.

Emission depletion is a nonlinear spectroscopic pump−probe method used for characterizing the ability of fluorescence inhibition. In contrast to transient absorption (TA) spectroscopy, in which the pump-induced change of the absorption of the probe pulse is measured, in this method the sample is excited by the pump pulse, and the change of the fluorescence intensity induced by the probe pulse is measured. Typically, the "turn-off" mechanism is stimulated emission,[18] although other mechanisms such as optical shelving[28] or ground-state-depletion (GSD)[29] have been exploited for manipulation of fluorescence. Emission depletion is routinely measured on organic dye molecules for subdiffraction limited microscopy applications (*e.g.*, STED microscopy),[19] but has rarely been employed with QDs.[24] As we show, this method has the advantages of clarifying the level structure of the system and its applicability for stimulated emission applications while being technically simple. It should be noted that observation of stimulated emission does not directly imply optical gain, since the loss induced by excited state absorption (ESA) impedes gain but is often inconsequential in the fluorescence depletion measurement.

The goal of this work is to gain better understanding of the characteristics of doped QDs in the context of stimulated emission. By probing the system when excited at different intensities, we obtain evidence for the dynamics of population inversion. A 4-level system, for example, would show a threshold for population inversion at very low excitation, whereas a 3-level system would require excitation of 50% of the population. Additionally, a 4-level system could exhibit full depletion of fluorescence by a probe depletion pulse, while a 3-level system would allow maximal fluorescence inhibition of 50% (or less, depending on the excited state population). Here we utilize emission depletion spectroscopy to show that the isovalently doped CdSe:Te system admits a 3-level behavior, with complete removal of the BX degeneracy. We then extend these measurements to CdS QDs with broadband trap-states emission, demonstrating that 3-level behavior is a general concept for QDs exhibiting emission involving a band-edge to trap state transition. Yet, our measurements reveal important differences between these two systems.

THEORETICAL MODEL

We apply a simple 3-level model to describe the CdSe:Te system. A schematic representation of the 3-level system is presented in Figure 1b. Further details can be found in the Supporting Information.

The assumptions of this model are that all MXs decay to the band-edge single exciton, which further decays to a trap state, all on a very short time scale. The radiative lifetime τ_r of the trap state is assumed to be long compared to all other time scales in the system.

The scheme of the model is described as follows. Population is excited with some probability P by an excitation pulse, and is being modified by a probe pulse. The probability of excitation to the biexciton state by the probe pulse is neglected. This is in stark contrast to the typical case of $\gamma = 2$ degeneracy of the lowest electronic excitation.[2]

The depletion ratio R_{dep} is defined according to

$$R_{dep} \equiv \frac{P(|t\rangle; \text{before probe pulse}) - P(|t\rangle; \text{after probe pulse})}{P(|t\rangle; \text{before probe pulse})}$$

$P(|t\rangle)$ is the probability for population of the trap state $|t\rangle$. This ratio is negative when the probe pulse induces further excitation, zero for no depletion, and approaches unity for full depletion. The parameters λ^{exc} and λ^{dep} denote the normalized energies $\lambda \equiv I/I_{sat}$ of the excitation (pump) and the depletion (probe) pulses, respectively, where I_{sat} is the saturation intensity of the transition.

In the strong excitation pulse limit $\lambda^{exc} \gg 1$, the dependence of the depletion ratio on the depletion pulse energy reduces to

$$R_{dep} = \left[1 - 0.5 \cdot \exp\left(\frac{\Delta t}{\tau_r}\right)\right] \cdot [1 - \exp(-\lambda^{dep})]$$

where Δt is the time delay between the pulses. The depletion ratio increases with the depletion pulse energy, saturating at a value of up to 50% (for $\Delta t \ll \tau_r$).

In the strong depletion pulse limit $\lambda^{dep} \gg 1$, the dependence of the depletion ratio on the excitation pulse energy reduces to

$$R_{dep} = 1 - \frac{0.5}{\exp\left(-\frac{\Delta t}{\tau_r}\right) \cdot [1 - \exp(-\lambda^{exc})]}$$

As the excitation energy is increased, a transition from absorption to stimulated emission is observed at an energy around I_{sat}^{exc},

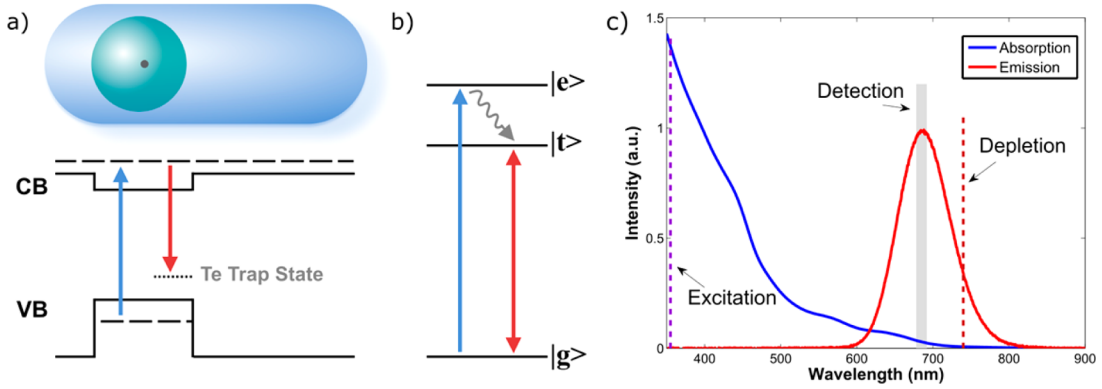

Figure 1. (a) Schematic illustration of the CdSe:Te/CdS core−shell nanorods, alongside their corresponding energy bands alignment. (b) Schematic description of the energy levels which constitute the 3-level system. The arrows depict the transitions of the band-edge absorption (blue) and the trap-related emission (red), respectively. (c) Absorption (blue) and emission (red) spectra of the Te-doped NRs. Also shown are the wavelengths chosen for the excitation (purple dashed line) and the depletion (dark red dashed line) pulses in the emission-depletion measurements, as well as the detection window (gray rectangle) of the fluorescence.

after which the depletion ratio saturates at the same value as in the previous limit.

RESULTS AND DISCUSSION

As potential candidates for a 3-level system, we studied Te-doped CdSe nanocrystal cores. The assumptions of the 3-level model are satisfied in this system: rapid relaxation of the electron and the hole to the band-edge (subpicosecond and picosecond time scales respectively),[14,30] followed by further fast relaxation of the hole to the Te-defect state on a subnanosecond time scale.[31] Additionaly, the long radiative lifetime of around 60 ns is much longer then all other relaxation time scales.

Figure 1a shows a schematic of the structure and band alignment of Te-doped CdSe core, overcoated by a CdS rod-like shell. Overcoating of the doped cores increases both the photostability and the quantum yield of the NRs, without significant modifaction of the band structure, which was shown to provide better conditions for observing gain.[8,32] The band-edge exciton absorption of these NRs appears at ∼650 nm, and emission from the Te defect states peaks at 688 nm. The Te trap states exhibit a large Stokes shift and spectraly broad emission, which allowed us to probe the transition between $|t\rangle$ and $|g\rangle$ without being influenced by the band-edge exciton state $|e\rangle$. Figure 1c shows the above band gap excitation wavelength and the depletion probe wavelength used in the measurement to be described. The depletion wavelength was tuned at the red-tail of the emission curve. The particular choice of depletion wavelength reflected a tradeoff between a large emission dipole moment of the Te-state related emission and having negligble absorption to the band-edge of thermally excited carriers in the ground state. Yet, the results presented here do not depend strongly on the exact depletion wavelength.

The experimental setup for emission depletion measurements is shown in Figure 2a. A 5 ns excitation pump pulse at 355 nm, and a 5 ns depletion probe pulse at 740 nm delayed by 20 ns from the excitation pulse, were focused into a cuvette containing the NRs dispersed in toluene. The 5 ns temporal width of the pulses is much longer than all cooling time-scales, therefore the saturation at the steady-state solution of the 3-level model when using strong pulses is justified. If one of the already excited charge carriers is further excited by the laser pulse, it decays on a comparably shorter time scale, much before the pulse ends. Therefore, this method is unaffected by such ESA. The effective waist of the excitation and depletion pulses at the focal plane was approximately 40 μm. Experimentally, however, it was found that maximal depletion ratios were obtained with strongly saturated excitation, better mimicking a flat-top excitation profile at a time delay of 20 ns, after multiply excited states have all relaxed.[33] This necessarily biases the energy densities used here toward higher values. Time-resolved fluorescence was collected at a right-angle, spectrally filtered by a monochromator, and detected by a photomultiplier tube with a time resolution of ∼2 ns. Further details of the experimental setup are described in the Methods section.

We compared decay time-traces of the fluorescence with and without the probe depletion pulse. The depletion ratio was defined as the normalized difference between the temporal integration of both curves after the depletion pulse, as shown in Figure 2b for a typical measurement.

We measured the Te-doped NRs depletion ratio's dependence on the energies of both the excitation pulse and the depletion pulse, as shown in Figure 3. In Figure 3a, the excitation pulse energy was fixed at a value above excitation saturation. This means that after ∼1 ns, all of the NRs are excited at the Te-defect state. The depletion ratio increases with depletion pulse energy, saturating at a value of around 0.3.

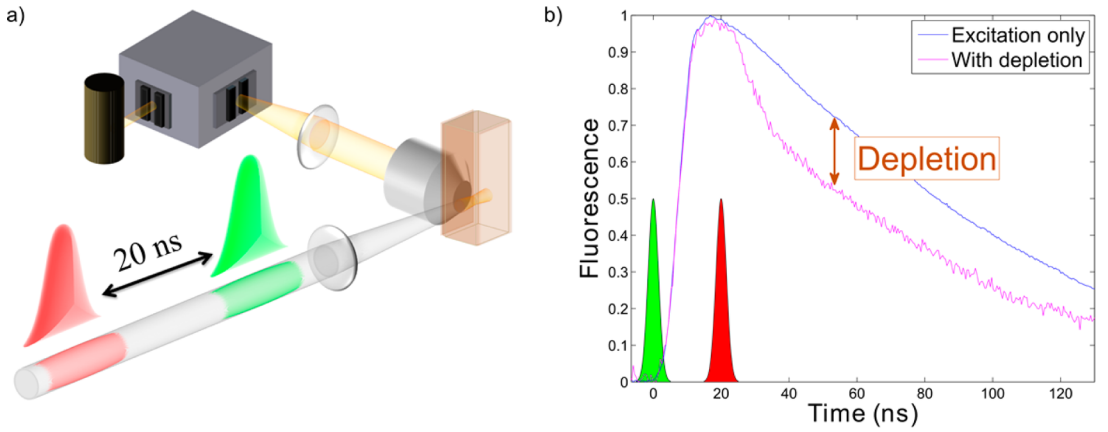

Figure 2. Schematic of the experimental setup (a) and a typical measured fluorescence time-trace (b). The fluorescence transient of the sample is measured after an excitation pulse and a delayed depletion pulse (magenta line), and compared to the transient after only an excitation pulse (blue line). The depletion ratio is defined as the normalized difference between the temporal integrations of both traces. Excitation (green) and depletion (red) pulses are also shown.

The data shows good agreement with the 3-level model, taking into account the 20 ns delay between the pulses. Since the time delay between the pump and the probe is of the order of the radiative lifetime, by the time the depletion pulse arrives, some of the QDs have already radiatively decayed. This accounts for a theoretically predicted value for the maximal depletion ratio of 0.29, in good agreement with the experimental observations.

In the experiments presented in Figure 3b, the depletion pulse energy was fixed at a value above depletion saturation. This means that a depletion pulse tuned to the $|t\rangle \leftrightarrow |g\rangle$ transition would leave the system at the steady-state of this pulse, namely, 50% of the population at the $|t\rangle$ state and 50% at the ground state. This plot shows the depletion ratio for different excitation pulse energies. At low excitations, most of the population is in the ground state, and the depletion pulse is absorbed and excites population to the $|t\rangle$ state, which is manifested by a *negative* depletion ratio. As the excitation energy was increased, we observed a clear transition from absorption to stimulated emission. This transition to stimulated emission was not observed in a control experiment on undoped type-I QDs, emphasizing the intrinsic modification induced by the Te doping (see Supporting Information). Figure 3 also shows the large difference of saturation energy densities between the $|t\rangle \leftrightarrow |g\rangle$ transition to the above band gap transition. The former is larger by one or 2 orders of magnitude compared to the latter, reflecting the much lower value of the dipole moment of the defect state transition compared to the band-edge transition.

Notably, despite the qualitative agreement, the quantitative agreement between the simple model and the results of Figure 3b is not as good. We attribute this to the fact that the model assumes flat-top beams, whereas in practice the excitation and probe pulses are both spatially nonuniform. Clearly, the results of Figure 3b, where the depletion ratio varies from negative to positive values, are more susceptible to distortion by this. Accounting for the spatial shape of the beams leads to a better quantitative agreement (not shown).

While the results of Figure 3 clearly show stimulated emission, they do not necessarily imply the observation of optical gain, due to the effects of excited state absorption as discussed above. To elucidate whether this system exhibits optical gain, we conducted transient absorption (TA) measurements on the Te-doped NRs. In this pump−probe configuration, a white probe pulse is used, and the difference in absorption between an optically excited medium and one which was not pre-excited is measured. These experiments were performed using a pump pulse at 520 nm, having a duration of 120 fs, a total energy of 3 μJ, and an effective size of about 500 μm. The negative differential absorption ($-\Delta$OD) spectrum of the probe pulse, taken ~1 ns after the pump, is shown (blue line) in Figure 4, and compared to the linear absorption spectrum (red line). Gain requires that the negative differential absorption exceeds the steady-state absorption (*i.e.*, the blue curve is higher than the red one). The decrease in absorption due to the pump pulse, manifested by positive peaks such as at the first excitonic peaks shown at ~650 nm and at ~575 nm in Figure 4, is likely a bleach signal due to the electronic excitation. An increase in absorption, associated with excited state absorption (manifested by a negative value) is observed at the red edge of the spectrum (λ > 750 nm). From the 3-level model and emission depletion measurements, we expect to observe optical gain at wavelengths used for the depletion pulse (~740 nm) when well above 50% the NRs are excited. From the TA data, it is likely that just about 50% of the NRs are excited by the pump (further pumping was not possible in our system due to the limited excitation pulse energy). This leads to *transparency* (zero absolute absorption) at

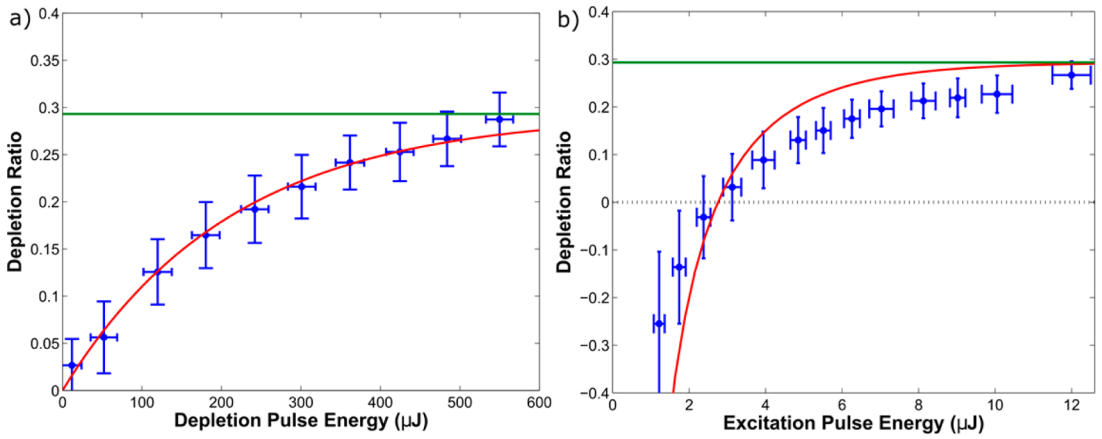

Figure 3. Emission depletion on Te-doped NRs. (a) Depletion ratio dependence on depletion pulse energy (blue points). Excitation pulses were of 12 μJ, above excitation saturation value. A clear saturation at around 0.3 depletion ratio is observed. The data is best fit to the 3-level model (red line) for depletion saturation energy of 212 μJ. (b) Depletion ratio dependence on excitation pulse energy (blue points). Depletion pulses energies were around 500 μJ, above depletion saturation value. The data is fit to the 3-level model (red line) for excitation saturation energy of 2.25 μJ. Notice the factor of ~100 between the two different saturation energies.

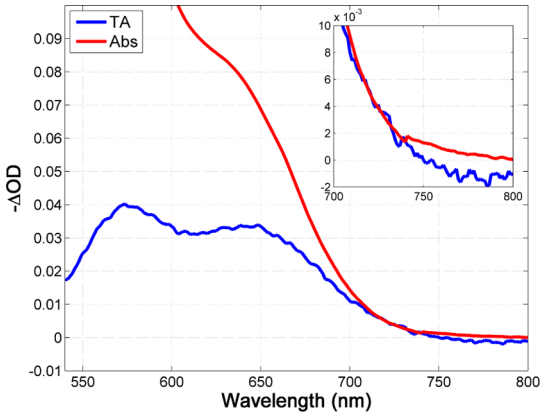

Figure 4. Transient absorption spectrum of Te-doped NRs (blue line), compared to their absorption spectrum (red line). Inset: Zero absolute absorption is observed at wavelengths around 730−740 nm.

wavelengths around 730−740 nm (Figure 4 inset), which suggests an upper bound of about ~ 1 mJ cm^{-2} for the threshold pumping level for population inversion.

As shown above, emission depletion measurements enable to clearly extract information about the energetics of an emitting trap state. They can provide not only details about the lifetime of the inverted population, but also direct spectroscopic evidence which can differentiate between an effective 3-level system and, for example, a 4-level one. One system where the level structure has recently been under debate is of broadband emitting CdS QDs. Similarly to the Te-doped NRs, these QDs also exhibit strong trap state related emission, although in this case the trap states arise due to poor passivation of the surface, and not as a result of a dopant site in the crystal. The spectrally broad surface-related emission, as well as the narrower higher energy band-edge transition, is clearly shown upon excitation in room temperature, as can be seen in Figure 5a. Surface-related photoluminescence in semiconducting QDs was traditionally treated as an unwanted side effect in colloidal syntheses, one which can usually be overcome by proper passivation of the surface. However, it can also be utilized as a means to generate energy-efficient illumination sources such as white LEDs.[34,35] The broadband surface related emission is often attributed to a broad distribution of the energies of trap states.[36,37] Recently, Mooney *et al.*[38] suggested an alternative explanation based on a semiclassical electron transfer (ET) model[39] to explain the broad and red-shifted surface-related emission, as well as its temperature dependence. The model evoked Marcus theory considerations to attribute the bandwidth of the trap-related emission to strong phonon coupling of the surface state. Here we utilize emission depletion spectroscopy to differentiate between these two models. For the multiple traps model, emission is to the ground state, hence a 3-level behavior is expected, whereas the electron transfer model predicts a phonon-broadened line where the emission is to an excited vibrational manifold of the ground state. Because of rapid phonon cooling, this should be equivalent to a 4-level scenario.

Emission depletion measurements were conducted on these QDs using the same experimental setup as for the Te-doped core−shell NRs. Figure 5b presents the dependence of the depletion ratio on the excitation energy. The observed 3-level-like trend bears similarity to the one measured for the doped NRs, where two features are clearly observed: a transition from absorption to population inversion, and saturation at the value predicted by the 3-level model. This appears to be inconsistent with the recently suggested semiclassical ET model. However, these results differ from the more "pure" 3-level behavior we witness in the case of the doped NRs. Here, the saturation of the depletion

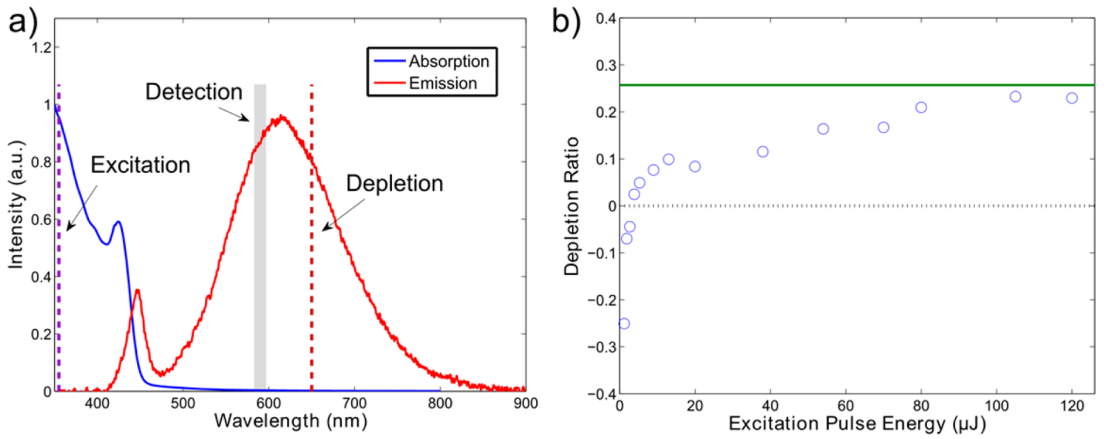

Figure 5. Emission depletion on broadband emitting CdS. (a) Absorption and photoluminescence spectra, showing both the band-edge and trap-states emission at 450 and 615 nm, respectively. Wavelengths of the excitation pulses (purple dashed line), the depletion pulses (dark red dashed line), and the detection window (gray rectangle) for the emission depletion measurements are also shown. (b) Dependence of the depletion ratio on excitation energy. The energy of the depletion pulses was fixed around 500 μJ, above depletion saturation value. The depletion ratio shows the same qualitative dependence on excitation energy as the doped NRs and as in the 3-level model.

ratio with the excitation energy is much slower, and extends over an energy scale larger by a factor of 10. The stepwise increase in the depletion ratio implies the presence of several saturation intensities. This can be attributed to a more complex multilevel structure within the band gap, either within the same dot or among different populations in the batch. The different surface related states have a wide distribution of cross sections for the transition from the ground state, which is manifested by the extended scale of saturation energies.

CONCLUSIONS

We performed emission depletion measurements on Te-doped NRs, in which the influence of a depletion pulse on excited NRs was studied. The Te dopants bind the lowest-energy excitons, and allow for huge biexciton blueshifts. Our measurements verify that this blueshift enables the complete removal of the exciton−biexciton degeneracy. Emission from these trap states showed behavior of a 3-level system, indicated by 50% threshold for population inversion and maximal depletion value predicted by a simple model.

Broadband emitting CdS QDs also exhibited clear 3-level system characteristics from emission depletion measurements. This is in contrast to a recently suggested model that predicted 4-level behavior. However, our results imply for the existence of a more complicated multilevel structure than that observed for the Te-doped NRs.

In both these systems, the existence of localized trap states within the band gap enabled population inversion in the single exciton regime for a band-edge to trap state transition. This results in what is, to the best of our knowledge, the longest-lived stimulated emission observed from colloidal quantum dots. Our findings indicate these systems are not suitable for STED microscopy, which requires complete depletion of fluorescence. However, Te-doped NRs in particular show high potential for light amplification applications.

METHODS

Synthesis. *Te-doped CdSe cores synthesis.* 26 mg of CdO, 120 mg of TDPA and 10 mL of ODE were degassed in a 50 mL flask under a vacuum at 120 °C for 30 min. The temperature was raised to 290 °C under argon flow and a mixture of 2 mL and 60 μL of 0.1 M Se:TOP and Te:TOP solutions (correspondingly) were injected to the flask. The reaction was stopped after 2−2.5 min. 2 mL of nonanoic acid were added upon cooling (at ∼100 °C).

CdSe(Te)-CdS rods synthesis. Purified CdSe(Te) dots were used as cores for the seeded-growth of CdS nanorods. 64 mg of CdO, 312 mg of ODPA, 82 mg of HPA and 3 g of TOPO were degassed in a 50 mL flask under a vacuum at 150 °C for 1 h. The temperature was raised to 350 °C under argon flow, and 2 mL of TOP were added upon dissolution of the CdO. At 350 °C, a solution of 120 mg S in 2 mL of TOP, mixed with 1 mL of CdSe(Te) in TOP was injected to the flask. The reaction was stopped after 5 min. 2 mL of nonanoic acid were added upon cooling (at ∼100 °C).

CdS QDs synthesis. 13 mg of CdO, 0.6 mL of oleic acid and 4 mL of ODE were degassed in a 50 mL flask under a vacuum at 110 °C for 1 h. The temperature was raised to 250 °C under argon flow, and 0.5 mL of 0.1 M S:ODE solution was injected. The reaction was stopped after 5 min.

TEM and Optical Characterization. TEM images of the QDs were taken at 120 kV, using a TEM (CM-120, Philips). UV−vis absorption spectra were measured using a UV−vis−NIR spectrophotometer (V-670, JASCO). PL spectra were measured using a spectrofluorimeter (USB4000, Ocean Optics).

Emission Depletion. Excitation and depletion pulses were generated by a frequency tripled Nd:YAG Q-switched laser oscillator pumping an optical parametric oscillator (OPO) (NT342/C/3/UVE, EKSPLA) with pulse durations of ∼5 ns at a repetition rate of 10 Hz. Excitation pulses at 355 nm were derived from third harmonic of the Nd:YAG. Depletion pulses at 740 nm, obtained from the OPO, were delayed using a ∼7 m delay line by 20 ns from the excitation pulses. Both beams were

merged by a dichroic mirror, then focused into a 10 × 10 mm rectangular quartz cuvette (Starna Cells), containing a solution of a low concentration of QDs dispersed in toluene. Fluorescence signals were collected at a right-angle by a 0.4 NA objective. After spectral filtering by a dielectric short-pass filter and a long-pass color glass, the signals were further passed through a monochromator (SpectraPro 2150i, Acton) for complete filtering of the laser pulses from the fluorescence. Time-resolved signals were measured by a photomultiplier tube (R10699, Hamamatsu Photonics, Hamamatsu City, Japan). Data was collected by a 600 MHz GHz oscilloscope (WaveSurfer 62Xs, Teledyne LeCroy). Pulse energies were measured by a pyroelectric sensor (PE9-C, Ophir Optronics). For measuring energies of single pulses synchronized with their corresponding fluorescence signals, beam samples were split from the laser lines by a glass slide. The beam samples were measured by another photomultiplier tube (R5108, Hamamatsu) connected to the oscilloscope, calibrated beforehand with a pyroelectric sensor.

Transient Absorption. Spectroscopy was performed using a system based on a mode-locked Ti:sapphire oscillator (MaiTai, Spectra Physics). The oscillator produces a train of <120 fs pulses (bandwidth ~10 nm fwhm), with a peak wavelength centered at 800 nm. The low-power oscillator pulses are amplified by a chirped pulse regenerative amplifier (CPA) (Spitfire ACE, Spectra Physics). The pulses are first stretched, then regeneratively amplified in a Ti:sapphire cavity, pumped by a pulsed Nd:YLF laser (Empower 45, Spectra Physics) operating at 1 kHz. After the pulse has been amplified and recompressed, its energy is about 5.0 μJ in a train of 1-kHz pulses, and about 1 μJ is used in the transient absorption setup. An independent pump pulse is obtained by pumping an optical parametric amplifier (OPA-800CF, Spectra Physics) that produces 120 fs pulses tunable from 300 nm to 3 μm. For these experiments the pump laser was tuned to 520 nm. The output power of the OPA is a few micro joules (depending on the chosen wavelength) at 1 kHz. The measurements are carried out in an EOS subnanosecond transient absorption spectrometer (Ultrafast Systems LLC), where the white light probe used is generated from a photonic crystal fiber laser. The pump and probe pulses are crossed in the sample at a small angle. The probe beam is imaged into an optical fiber which is then coupled to the spectrograph. Part of the probe beam is collected directly to another spectrograph, as a reference, in order to reduce noise in the measurement. The pump power intensities were measured using a photodiode sensor (Ophir Optronics) in proximity to the sample.

Conflict of Interest: The authors declare no competing financial interest.

Acknowledgment. The authors acknowledge financial support from the Israeli centers of research excellence program, the Leona M. and Harry B. Helmsley charitable trust and the European Research Council (starting investigator grant SINSLIM 258221). O.L., N.M. and I.P. performed the optical experiments. Nanoparticles were synthesized and characterized by N.M. The work was conceived and supervised by D.O.

Supporting Information Available: A more detailed account of synthetic procedures, theoretical calculations, control emission depletion measurements on undoped type-I QDs. This material is available free of charge *via* the Internet at http://pubs.acs.org.

REFERENCES AND NOTES

1. Giessen, H.; Woggon, U.; Fluegel, B.; Mohs, G.; Hu, Y. Z.; Koch, S. W.; Peyghambarian, N. Femtosecond Optical Gain in Strongly Confined Quantum Dots. *Opt. Lett.* **1996**, *21*, 1043–1045.
2. Klimov, V. I.; Mikhailovsky, A. A.; Xu, S.; Malko, A.; Hollingsworth, J. A.; Leatherdale, C. A.; Eisler, H.-J.; Bawendi, M. G. Optical Gain and Stimulated Emission in Nanocrystal Quantum Dots. *Science* **2000**, *290*, 314–317.
3. Kazes, M.; Lewis, D. Y.; Ebenstein, Y.; Mokari, T.; Banin, U. Lasing from Semiconductor Quantum Rods in a Cylindrical Microcavity. *Adv. Mater.* **2002**, *14*, 317–321.
4. Chan, Y.; Steckel, J. S.; Snee, P. T.; Caruge, J. M.; Hodgkiss, J. M.; Nocera, D. G.; Bawendi, M. G. Blue Semiconductor Nanocrystal Laser. *Appl. Phys. Lett.* **2005**, *86*, 073102.
5. Cooney, R. R.; Sewall, S. L.; Sagar, D. M.; Kambhampati, P. State-Resolved Manipulations of Optical Gain in Semiconductor Quantum Dots: Size Universality, Gain Tailoring, and Surface Effects. *J. Chem. Phys.* **2009**, *131*, 164706.
6. Grim, J. Q.; Christodoulou, S.; Di Stasio, F.; Krahne, R.; Cingolani, R.; Manna, L.; Moreels, I. Continuous-Wave Biexciton Lasing at Room Temperature Using Solution-Processed Quantum Wells. *Nat. Nanotechnol.* **2014**, *9*, 891–895.
7. Rossetti, R.; Ellison, J. L.; Gibson, J. M.; Brus, L. E. Size Effects in the Excited Electronic States of Small Colloidal CdS Crystallites. *J. Chem. Phys.* **1984**, *80*, 4464–4469.
8. Kazes, M.; Oron, D.; Shweky, I.; Banin, U. Temperature Dependence of Optical Gain in CdSe/ZnS Quantum Rods. *J. Phys. Chem. C* **2007**, *111*, 7898–7905.
9. Hoogland, S. Optical Gain and Lasing in Colloidal Quantum Dots. In *Colloidal Quantum Dot Optoelectronics and Photovoltaics*; Konstantatos, G., Sargent, E. H., Eds.; Cambridge University Press: New York, 2013.
10. Sewall, S. L.; Franceschetti, A.; Cooney, R. R.; Zunger, A.; Kambhampati, P. Direct Observation of the Structure of Band-Edge Biexcitons in Colloidal Semiconductor CdSe Quantum Dots. *Phys. Rev. B: Condens. Matter Mater. Phys.* **2009**, *80*, 081310.
11. Kambhampati, P. Multiexcitons in Semiconductor Nanocrystals: A Platform for Optoelectronics at High Carrier Concentration. *J. Phys. Chem. Lett.* **2012**, *3*, 1182–1190.
12. Cooney, R. R.; Sewall, S. L.; Sagar, D. M.; Kambhampati, P. Gain Control in Semiconductor Quantum Dots *via* State-Resolved Optical Pumping. *Phys. Rev. Lett.* **2009**, *102*, 127404.
13. Dias, E. A.; Saari, J. I.; Tyagi, P.; Kambhampati, P. Improving Optical Gain Performance in Semiconductor Quantum Dots *via* Coupled Quantum Shells. *J. Phys. Chem. C* **2012**, *116*, 5407–5413.
14. Klimov, V. I.; Mikhailovsky, A. A.; McBranch, D. W.; Leatherdale, C. A.; Bawendi, M. G. Quantization of Multiparticle Auger Rates in Semiconductor Quantum Dots. *Science* **2000**, *287*, 1011–1013.
15. Klimov, V. I.; Ivanov, S. A.; Nanda, J.; Achermann, M.; Bezel, I.; McGuire, J. A.; Piryatinski, A. Single-Exciton Optical Gain in Semiconductor Nanocrystals. *Nature* **2007**, *447*, 441–446.
16. Dang, C.; Lee, J.; Breen, C.; Steckel, J. S.; Coe-Sullivan, S.; Nurmikko, A. Red, Green and Blue Lasing Enabled by Single-Exciton Gain in Colloidal Quantum Dot Films. *Nat. Nanotechnol.* **2012**, *7*, 335–339.
17. Grivas, C.; Li, C.; Andreakou, P.; Wang, P.; Ding, M.; Brambilla, G.; Manna, L.; Lagoudakis, P. Single-Mode Tunable Laser Emission in the Single-Exciton Regime from Colloidal Nanocrystals. *Nat. Commun.* **2013**, *4*, 2376.
18. Hell, S. W.; Wichmann, J. Breaking the Diffraction Resolution Limit by Stimulated Emission: Stimulated-Emission-Depletion Fluorescence Microscopy. *Opt. Lett.* **1994**, *19*, 780–782.
19. Hell, S. W. Far-Field Optical Nanoscopy. *Science* **2007**, *316*, 1153–1158.
20. Resch-Genger, U.; Grabolle, M.; Cavaliere-Jaricot, S.; Nitschke, R.; Nann, T. Quantum Dots *versus* Organic Dyes as Fluorescent Labels. *Nat. Methods* **2008**, *5*, 763–775.
21. Irvine, S. E.; Staudt, T.; Rittweger, E.; Engelhardt, J.; Hell, S. W. Direct Light-Driven Modulation of Luminescence from Mn-Doped ZnSe Quantum Dots. *Angew. Chem.* **2008**, *120*, 2725–2728.
22. Hoyer, P.; Staudt, T.; Engelhardt, J.; Hell, S. W. Quantum Dot Blueing and Blinking Enables Fluorescence Nanoscopy. *Nano Lett.* **2010**, *11*, 245–250.
23. Bang, J.; Park, J.; Velu, R.; Yoon, E.; Lee, K.; Cho, S.; Cha, S.; Chae, G.; Joo, T.; Kim, S. Photoswitchable Quantum Dots by Controlling the Photoinduced Electron Transfers. *Chem. Commun.* **2012**, *48*, 9174–9176.
24. Lesoine, M. D.; Bhattacharjee, U.; Guo, Y.; Vela, J.; Petrich, J. W.; Smith, E. A. Subdiffraction, Luminescence-Depletion

Imaging of Isolated, Giant, CdSe/CdS Nanocrystal Quantum Dots. *J. Phys. Chem. C* **2013**, *117*, 3662–3667.
25. Ivanov, S. A.; Nanda, J.; Piryatinski, A.; Achermann, M.; Balet, L. P.; Bezel, I. V.; Anikeeva, P. O.; Tretiak, S.; Klimov, V. I. Light Amplification Using Inverted Core/Shell Nanocrystals: Towards Lasing in the Single-Exciton Regime. *J. Phys. Chem. B* **2004**, *108*, 10625–10630.
26. Avidan, A.; Oron, D. Large Blue Shift of the Biexciton State in Tellurium Doped CdSe Colloidal Quantum Dots. *Nano Lett.* **2008**, *8*, 2384–2387.
27. Zhang, L.; Lin, Z.; Luo, J. W.; Franceschetti, A. The Birth of a Type-II Nanostructure: Carrier Localization and Optical Properties of Isoelectronically Doped CdSe: Te Nanocrystals. *ACS Nano* **2012**, *6*, 8325–8334.
28. Bretschneider, S.; Eggeling, C.; Hell, S. W. Breaking the Diffraction Barrier in Fluorescence Microscopy by Optical Shelving. *Phys. Rev. Lett.* **2007**, *98*, 218103.
29. Hell, S. W.; Kroug, M. Ground-State-Depletion Fluorescence Microscopy: A Concept for Breaking the Diffraction Resolution Limit. *Appl. Phys. B: Laser Opt.* **1995**, *60*, 495–497.
30. Kambhampati, P. Hot Exciton Relaxation Dynamics in Semiconductor Quantum Dots: Radiationless Transitions on the Nanoscale. *J. Phys. Chem. C* **2011**, *115*, 22089–22109.
31. Avidan, A.; Pinkas, I.; Oron, D. How Quickly Does a Hole Relax into an Engineered Defect State in CdSe Quantum Dots. *ACS Nano* **2012**, *6*, 3063–3069.
32. Htoon, H.; Hollingworth, J. A.; Malko, A. V.; Dickerson, R.; Klimov, V. I. Light Amplification in Semiconductor Nanocrystals: Quantum Rods *versus* Quantum Dots. *Appl. Phys. Lett.* **2003**, *82*, 4776–4778.
33. Oron, D.; Kazes, M.; Shweky, I.; Banin, U. Multiexciton Spectroscopy of Semiconductor Nanocrystals under Quasi-Continuous-Wave Optical Pumping. *Phys. Rev. B: Condens. Matter Mater. Phys.* **2006**, *74*, 115333.
34. Krause, M. M.; Mooney, J.; Kambhampati, P. Chemical and Thermodynamic Control of the Surface of Semiconductor Nanocrystals for Designer White Light Emitters. *ACS Nano* **2013**, *7*, 5922–5929.
35. Nizamoglu, S.; Mutlugun, E.; Akyuz, O.; Perkgoz, N. K.; Demir, H. V.; Liebscher, L.; Sapra, S.; Gaponik, N.; Eychmüller, A. White Emitting CdS Quantum Dot Nanoluminophores Hybridized on Near-Ultraviolet LEDs for High-Quality White Light Generation and Tuning. *New J. Phys.* **2008**, *10*, 023026.
36. Chestnoy, N.; Harris, T. D.; Hull, R.; Brus, L. E. Luminescence and Photophysics of Cadmium Sulfide Semiconductor Clusters: The Nature of the Emitting Electronic State. *J. Phys. Chem.* **1986**, *90*, 3393–3399.
37. Hässelbarth, A.; Eychmüller, A.; Weller, H. Detection of Shallow Electron Traps in Quantum Sized CdS by Fluorescence Quenching Experiments. *Chem. Phys. Lett.* **1993**, *203*, 271–276.
38. Mooney, J.; Krause, M. M.; Saari, J. I.; Kambhampati, P. Challenge to the Deep-Trap Model of the Surface in Semiconductor Nanocrystals. *Phys. Rev. B: Condens. Matter Mater. Phys.* **2013**, *87*, 081201.
39. Jortner, J. Temperature Dependent Activation Energy for Electron Transfer between Biological Molecules. *J. Chem. Phys.* **1976**, *64*, 4860–4867.